Cement and Concrete Research 101 (2017) 102–113

Contents lists available at ScienceDirect

Cement and Concrete Research

journal homepage: www.elsevier.com/locate/cemconres

Solute transport solved with the Nernst-Planck equation for concrete pores with 'free' water and a double layer

C.A.J. Appelo

Valeriusstraat 11, NL 1071MB Amsterdam, The Netherlands

ARTICLE INFO

Keywords:
Concrete
Diffusion
Pore solution
Electro-mediated transport
Chloride

ABSTRACT

For calculating ion transport in electro-migration experiments in concrete, the pore space is divided between free pore water and a double layer that compensates the surface charge of minerals lining the pore. The concentrations of counter-ions and co-ions in the double layer are averaged in a Donnan layer, which allows to solve the flux equation of the individual ions. A numerical model is developed for transient states, with the harmonic mean of the chemical activity coefficients and the physical parameters to adapt cell sizes in zones with high concentration gradients. Diffusion coefficients of the ions are corrected for temperature and ionic strength with an empirical equation with three parameters optimized on published transport numbers and specific conductances. The current and the Cl^- breakthrough is calculated in an electro-migration experiment with a concrete sample. The surface charge is positive in the experiment, enhancing and reducing the diffusivity of anions and cations.

1. Introduction

The application of an electrical potential gradient of a few hundred V/m on a concrete sample enhances the diffusion of charged species by orders of magnitude and facilitates the determination of the diffusion coefficient of Cl^- and other species in concrete samples. Analytical and numerical models can be used to extract the transport properties from the electrical current or by analyzing the Cl^- throughput [1–3]. However, to model both the Cl^- breakthrough and the current is still a challenge, as can be illustrated with an experiment by Friedmann et al. [4] shown in Fig. 1. In the experiment, a concrete sample was cured and equilibrated with Na, KOH solution, and the same solution was placed in the anode and cathode reservoirs at the column ends. A 3 V gradient was applied over the 1 cm sample, and, after 44 h, NaCl was added to the cathode reservoir. The current falls when NaCl is added, and increases again a few hours later. Fig. 1 shows the measured current density and the Cl^- increase in the anode reservoir over time, and model calculations with the Nernst-Planck equation.

The Cl^- increase in the anode reservoir allows to calculate the effective diffusion coefficient of Cl^-, $D_{e,Cl} = D_{w,Cl} \times \varepsilon / G$, where ε is the porosity, D_w is the diffusion coefficient in water, and G is the geometrical factor that corrects for the tortuosity of the porous medium. Alternatively, the current can be used to find these transport properties [2,4,6,7]. The resulting D_e values (in 10^{-12} m^2/s) for the experiment shown in Fig. 1 are 25.6 ([4], Eq. (15)), 23.5 [5], and 12.7 [2]. Unfortunately, such differences are not uncommon and the incorrect number can permeate through the literature [3].

In Fig. 1, the full and dashed lines are calculated with Krabbenhøft and Krabbenhøft's number for ε / G, and the increase of Cl^- is well modeled. However, the calculations were done with porosity of 1, thus, with the apparent diffusion coefficient. If carried out with a porosity of 0.24 (obtained by Narsilio et al., [2]) and the geometrical factor is adapted to keep $D_{e,Cl} = 23.5 \times 10^{-12}$ m^2/s, the current density is the same in the first 44 h since the system in that period is in steady state with a uniform Na,KOH solution throughout. However, when NaCl is added, the current change and the Cl^- breakthrough arrive four times earlier because the geometrical factor is four times smaller (model lines with $\varepsilon = 0.24$ in Fig. 1). For transient conditions, the water-filled porosity must be used in a numerical model, and the effective diffusion coefficient may be more in line with Narsilio's number.

On the other hand, the modeled current is smaller than measured, which suggests that the factor ε / G is higher. In that case, Cl^- would arrive even earlier, and the breakthrough is then retarded by sorption or ion exchange [8–10], or by mass-exchange with stagnant or unconnected water [11–16] since the capillary porosity, for the $w/c = 0.7$ ratio in this experiment, may be higher than 0.24 [17]. In addition, when comparing current and Cl^- breakthrough, the changes of the diffusion coefficients with solution composition and the accompanying variations of the transport numbers (the fraction of the current carried by the ions) must be accounted for [18,19].

Before discussing the details needed for modeling, it is helpful to consider what happens in the experiment shown in Fig. 1. First, when

E-mail address: appt@hydrochemistry.eu.

http://dx.doi.org/10.1016/j.cemconres.2017.08.030
Received 23 February 2017; Received in revised form 25 May 2017; Accepted 29 August 2017
Available online 14 September 2017

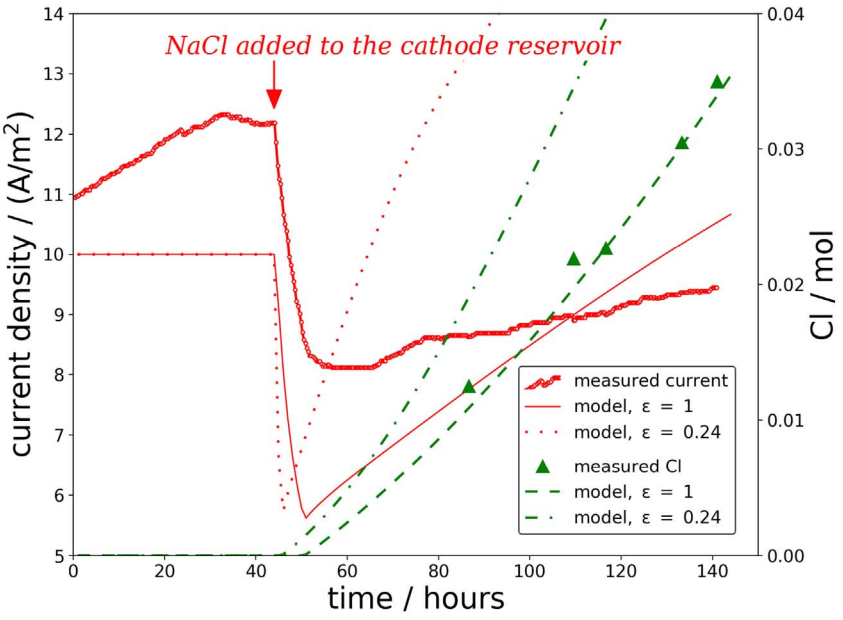

Fig. 1. Current density and Cl increase in the anode reservoir in Friedmann's [4] experiment with $w/c = 0.7$. The model lines are calculated with the parameters from Krabbenhøft and. Krabbenhøft [5] ($\varepsilon/G = 0.0116$, $\varepsilon = 1$) and with porosity $\varepsilon = 0.24$ from Narsilio et al. [2] ($\varepsilon/G = 0.0116$).

the potential is applied on the sample, the modeled current remains constant, whereas the measured current increases with time, probably as result of chemical reactions of cement minerals [20,21]. Dissolution of portlandite is relatively quick [22–24], which increases the concentrations of Ca^{2+} and OH^- in the pore water and thus, the current. But, if the dissolution reaches equilibrium too quickly, the Ca^{2+} and OH^- concentrations are fixed in the column, providing steady state conditions that will not produce the gradual current increase in time that the experiments show.

Second, when NaCl is added to the cathode reservoir, the current falls, and the reason is known [4,5]: Cl^- enters the column by both the concentration- and the electric potential-gradient, while the diffusion of Na^+ is counter to the electric potential-gradient. This implies that, in the beginning, the total anion concentration is limited by the original cation concentrations in the column. The conductivity is reduced when OH^- is partially replaced by Cl^- while the total anion concentration remains the same because Cl^- has a smaller diffusion coefficient than OH^- (see [5] for instructive calculations). When the Cl^- front arrives at the anode-end, the current cannot go down further, but it can increase because a slow diffusion of Na^+ augments the total concentrations in the column. Fig. 1 shows that the model overestimates the increase rate of the current density in that part of the experiment.

One possible explanation for the much slower increase rate of Na^+ is exclusion of cations from part of the pore space [5,25]. Ion exclusion originates from the surface charge of minerals, which creates an electrical double layer in the pores in which counter-ions accumulate and co-ions are excluded relative to 'free' water that is charge-neutral. Of the major cement minerals, AFm is an anion exchanger [26,27] and portlandite sorbs Cl^-, at least when the concentration is below 1 M NaCl [9], and these minerals have a positive surface charge at the pH of the experiment [9]. The surface charge on CSH is primarily a function of the Ca^{2+} activity, with the isoelectric point (where the surface is without charge) attained when the Ca^{2+} activity is about 0.0015 [28], and this mineral probably has a negative surface charge in the experiment. Exclusion of cations means that the pore circumference is positively charged, and that the concentration of OH^- is higher in the electrical double layer than in 'free' pore water. A higher concentration of OH^- in the concrete pores may explain the higher measured than modeled current, and a model for calculating it is the subject of this paper.

The proposed model uses the Nernst-Planck equation for calculating the flux, which accounts for the effects of both chemical-potential and electrical-potential gradients in transport processes. For the steady state, the calculations can be done by hand. For transient states, the equation is solved with finite differences, programmed in PHREEQC [29], with the non-linear distribution of the electrical potential obtained from Ohm's law. Furthermore, parameters are derived for calculating the temperature and ionic strength dependence of the transport numbers of individual ions. The model is applied to calculate the current and Cl^- breakthrough in Friedmann's experiment.

2. Finite difference solution for electro-migration

The Nernst-Planck equation for the flux of a solute species is:

$$J_i = -D_i\left(\frac{dc_i}{dx} + c_i\frac{d\ \ln\gamma_i}{dx} + z_i c_i\frac{F}{RT}\frac{d\psi}{dx}\right) \quad (1)$$

where J_i is the flux of solute i (mol/m^2/s), D_i is the diffusion coefficient in the solution (m^2/s), c is the concentration (mol/m^3), x is the distance (m), γ is the activity coefficient (−), z_i is the charge number of i (−), F is the Faraday constant (96 485 C/eq), R is the gas constant (8.3145 V·C/eq/K), T is the absolute temperature (K), and ψ is the electrical potential (V). Chemical models use molality (mol/kg H_2O) as the temperature- and pressure-independent concentration unit, here assumed numerically equal to molarity (mol/dm^3) that is in the flux equation.

In transient states, the concentrations change by:

$$\frac{\partial c_i}{\partial t} = \frac{\partial J_i}{\partial x} - \frac{\partial q_i}{\partial t} \quad (2)$$

where q_i is the concentration in the solid (mol/m^3 H_2O), which changes as a result of mineral reactions, sorption and ion exchange, and exchange with stagnant zones.

2.1. Concentrations in free and charged pore water

If the pores are lined with minerals that have a surface charge, the concentrations of the charged ions vary gradually from the surface, and the value for c_i in Eq. (1) varies accordingly. Appelo and Wersin [30] simplified the resulting complications for a transport model by subdividing the pore into a charge-neutral, 'free' water part, and a Donnan layer as shown in Fig. 2.

The concentrations in the Donnan layer are a function of the concentrations in the free pore water and the surface charge that must be

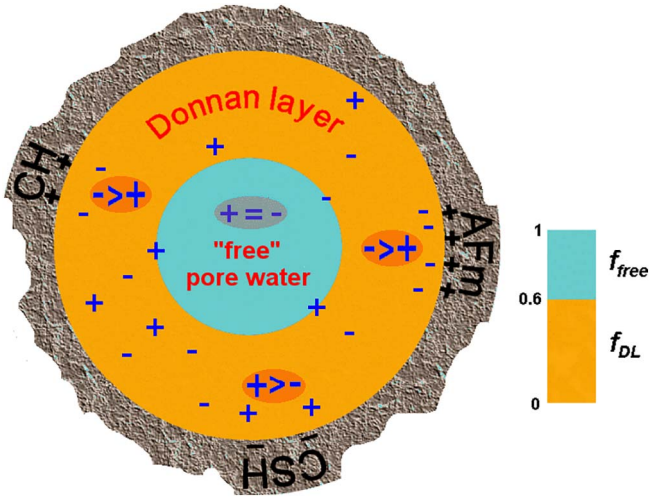

Fig. 2. Dividing the pore space in concrete into two fractions:
f_{free}, uncharged pore water, and
f_{DL}, a Donnan layer (DL) that neutralizes the surface charge of concrete minerals.

neutralized. The charge balance in free pore water is:

$$\sum z_i c_{free,i} = 0 \tag{3}$$

In the Donnan layer the charge balance is:

$$\sum z_i c_{DL,i} v_{DL} + Su = 0 \tag{4}$$

where v_{DL} is the volume of the Donnan layer (m^3, taken equal to Mg water), and Su is the surface charge (mol). The concentrations in free water and the Donnan layer are related by the Boltzmann equation:

$$c_{DL,i} = c_{free,i} \exp\left(\frac{-z_i F \psi_{DL}}{RT}\right) = c_{free,i} g_{DL,i} \tag{5}$$

where ψ_{DL} is the potential in the Donnan layer (V). Inserting Eq. (5) in Eq. (4) allows to find ψ_{DL} for given c_{free} and Su values, and then, to obtain the concentrations in the Donnan layer.

2.1.1. Illustration: calculating sorbed Na^+ from concentrations in the Donnan layer

When, in an experiment, water is removed from a suspension by centrifuging or filtrating, the ions in the Donnan layer are part of what is 'sorbed'. The quotient of the excess moles in the Donnan layer and the moles in the solution can be compared with measured distribution coefficients, and it is of interest to also compare the Donnan simplification with results obtained by integrating the concentrations in the electrical double layer using the Gouy-Chapman equations.

For example, the distribution coefficient of Na^+ on CSH [31] can be modeled following the approach of Haas and Nonat [32–34 Fig. 8], taking $C_{0.83}SH$ for which the solubility is well-established [35], add a surface complexation model [28], CaO to increase C/S to the 0.85 of the experiment, and then react it with 0.3 M NaOH solution (Table 1).

At the high pH of the NaOH solution, the surface complex Si_OH dissociates and associates with Ca^{2+} into Si_OCa^+, thus lowering the solute concentration of Ca^{2+}. This enhances the dissolution of CSH by orders of magnitude and the silicate anions contribute significantly to the alkalinity. The major ions in solution are Na^+, OH^-, and $H_2SiO_4^{2-}$ (Table 1) and their concentrations were calculated as a function of distance from the surface with matlab template files ([36], p. 293), or with the Donnan option using PHREEQC. In all cases, the concentrations in the double layer balance the same negative charge of −44.7 meq/L on the surface.

The traditional Gouy-Chapman picture is presented in Fig. 3A, with concentrations from the surface ($x = 0$) to the point where the potential is virtually 0. The Gouy-Chapman equation for the potential at the surface is:

$$\psi_0 = \text{asinh}\left(\frac{F\sigma}{0.117 I_s^{0.5}}\right) \times \left(\frac{2RT}{F}\right) = -0.077 \text{ V} \tag{6}$$

where Fσ is the surface charge (C/m^2) and I_s is the ionic strength (mol/L). However, the equation is for single-charged ions and the ionic strength has been introduced conventionally as a general measure of the concentrations [36, p. 292]. The presence of a small concentration of the double-charged silicate anion requires adjustment of ψ_0 to −0.078 V for balancing the surface charge in Fig. 3A. It can be noted that the concentration of the anions and of Na^+ decreases and increases, respectively, towards the surface, demonstrating that the surface charge is balanced by a surplus of counter-ions (Na^+ is 'sorbed') and a deficit of co-ions (which are 'negatively sorbed'). At the surface, the Na^+ concentration is unlikely high since the ions are considered to be point charges.

Fig. 3B shows the results when an ion-size parameter is introduced that limits the approach to the surface (here equal to the ion-size parameter (a) in the Debye-Hückel equation), and when integrating over 2 Debye lengths, $n_D = 2$ [37], from the smallest $a = 0.35$ nm for OH^-.

The Debye length ($m^{-1}(mol/L)^{-0.5}$) is:

$$\kappa = \frac{1}{F}\sqrt{\frac{\varepsilon_w RT}{2 \times 10^3 I_s}} \tag{7}$$

where ε_w is the dielectric permittivity of water (6.94×10^{-10} F/m at 25 °C).

This case needs, for balancing the surface charge, $\psi_0 = -0.085$ V. Fig. 3C presents the concentrations of the Donnan model with $n_D = 2$.

The concentrations in the double layer in Fig. 3A and B can be integrated to an average concentration $c_{DL,i}$ like the one for the Donnan layer, and the overall concentration in a volume that contains fractions of free water and electrical double layer water is:

$$c_i = f_{free} c_{free} + (1 - f_{free}) c_{DL,i} \tag{8}$$

where c_i is equal here and in the Nernst-Planck equation.

In the example, $c_{Na^+} = 296$ mM, equal to NaOH added. The input-variables are $c_{free,\ Na^+} = 259$ mM and a surface charge of −44.7 mM, and thus, (296 – 259 + −44.7) = −7.7 mM is balanced by negative sorption of anions. The calculated overall concentrations of Na^+ are identical to the expected number in all three cases, within the accuracy of the integration. Thus, the Donnan simplification will give the same result for the c term in the Nernst-Planck equation as the numerical integrations, while being much more stable and much less time-consuming.

Finally, Fig. 3D shows the measured distribution coefficients for Na^+ and calculated with the Donnan model. The calculated distribution coefficient follows from Eq. (8):

$$K_{d,\text{Na}} = \frac{(1-f_{free})(c_{DL,\text{Na}} - c_{free,\text{Na}})}{c_{free,\text{Na}}} \times \frac{mL\ H_2O}{g\ CSH} \tag{9}$$

The K_d has been calculated with 2 and 0.02 Debye lengths for the thickness of the double layer. The first case is representative for CSH in suspension in Hong and Glasser's experiment, the second one can refer to CSH from which external water has been removed, leaving the counter–ions only. The distribution coefficient of Na^+ is higher than in the first case where the negative adsorption of anions contributes to charge-balancing.

The trend of the modeled K_d with Na^+ concentration is to start small, increase to a maximum at 15–30 mM NaOH, and decrease at higher concentrations. It follows the reactions at the surface and the concentrations of Ca^{2+} and Na^+ in solution. At low Na^+ concentration, Ca^{2+} balances the surface charge. When the Na^+ concentration and the pH increase, Ca^{2+} is complexed on the surface and Na^+ takes over. The increase of the Si_OCa^+ complex with increasing pH decreases the

Table 1
Equilibria, reactions and calculated concentrations for the experiment of Hong and Glasser [31] in which CSH dissolves in 0.3 M NaOH solution.

Equilibria and reactions	log *K*	mmol/L
$(CaO)_{0.83}SiO_2(H_2O)_{0.97}$ + 0.86 H_2O = 0.83 Ca^{2+} + $H_3SiO_4^-$ + 0.66 OH^-	−8.0[a]	534
Si_OH = Si_O^- + H^+	−12.3[b]	266
Si_OH + Ca^{2+} = Si_OCa^+ + H^+	−9.4[b]	
CaO + 2 H^+ → Ca^{2+} + H_2O		0.31
NaOH → Na^+ + OH^-		296

Concentrations (mmol/L)

	OH^-	Na^+	Na^+_{sorbed}	$H_2SiO_4^{2-}$	$H_3SiO_4^-$	(Ca^{2+} + $CaOH^+$)	(Si_O^- − Si_OCa^+)
experiment[c]	247[d]	236	60			0.09	
calculated[e]	232	259	37	11.4	4.3	0.008	−44.7[f]

[a] Lothenbach et al. [35].
[b] Viallis-Terrisse et al. [28], 4.8 sites/nm^2, surface area 500 m^2/g CSH.
[c] Hong and Glasser [31], 66.7 g CSH/L water, CSH with 14% water.
[d] The titration of OH^- probably includes silicate anions.
[e] Calculated with PHREEQC [29].
[f] The surface charge is $F\sigma = -44.7 \times 10^{-3}$ F / (500 × 66.7) = −0.129 C/m^2.

surface charge, so that less Na^+ enters the double layer and K_d decreases. The measured data seem to confirm the model trend, but the measured K_d's are somewhat higher than modeled. However, the surface complexation model is based on CSH that shows a distinct X-ray pattern [28], whereas CSH in the experiment is amorphous. It is not unlikely that the surface sites are higher in the amorphous form, which can explain the higher observed K_d.

2.2. Harmonic mean solution of the parameters in the transport equation

The Nernst-Planck equation can be solved with a split-operator scheme in which, for a time step, first diffusive transport is calculated with central differences, and then the chemical reactions [36]. For the transport part, the diffusion coefficients are corrected for geometric properties of the porous medium, and the mass transfer is obtained by multiplying with the surface area available for diffusion. When these physical properties vary from cell to cell, the mass transfer can be compared inside two cells j and k towards the interface jk:

$$M_{i,j} = -\frac{\varepsilon_j A_j}{G_j} D_i \left(\frac{(c_{i,jk} - c_{i,j})\left(1 + \frac{1n\gamma_{i,jk} - 1n\gamma_{i,j}}{1nc_{i,jk} - 1nc_{i,j}}\right) + z_i c_{i,j} \frac{F}{RT}(\psi_{jk} - \psi_j)}{x_j/2} \right) \tag{10}$$

and

$$M_{i,k} = -\frac{\varepsilon_k A_k}{G_k} D_i \left(\frac{(c_{i,k} - c_{i,jk})\left(1 + \frac{1n\gamma_{i,k} - 1n\gamma_{i,jk}}{1nc_{i,k} - 1nc_{i,jk}}\right) + z_i c_{i,k} \frac{F}{RT}(\psi_k - \psi_{jk})}{x_k/2} \right) \tag{11}$$

where M_i is the mass transfer of solute i (mol/s), ε_j is the porosity of cell j (−), A is the surface area of the cell (m^2), G is the geometrical factor that relates the diffusion coefficient in pure water and in the porous medium (−), $c_{i,j}$ is the concentration in cell j (mol/m^3), x is the cell-length (m), and subscript $_{jk}$ indicates the interface of cells j and k. At steady state, $M_{i,j} = M_{i,k}$, which permits to solve for $c_{i,\,jk}$. The result is that the harmonic mean of the cells' properties appears in the equation that gives the mass transfer from cell j to k:

$$M_i = -D_i \frac{b_j b_k}{b_j + b_k} \left((c_{i,k} - c_{i,j}) a_{i,k-j} + z_i \overline{c_{i,jk}} \frac{F}{RT} (\psi_k - \psi_j) \right) \tag{12}$$

where $a_{i,k-j}$ is the correction for activity coefficients,

$$a_{i,k-j} = 1 + \frac{\ln \gamma_{i,k} - \ln \gamma_{i,j}}{\ln c_{i,k} - \ln c_{i,j}} \tag{13}$$

where b_j and b_k are defined by the cell lengths and the bipartite division of the pore space into free and Donnan water with Eqs. (5) and (8),

$$b_j = \frac{2\varepsilon_j A_j}{G_j x_j} \left(f_{free} + (1 - f_{free}) \frac{g_{DL,i}}{\eta_{rDL}} \right)_j \tag{14}$$

and similarly for b_k, where f_{free} is the fraction of free pore water,

$$f_{free} = \nu_{free}/(\nu_{free} + \nu_{DL}) \tag{15}$$

and finally,

$$\varepsilon_j A_j = (\nu_{free} + \nu_{DL})_j / x_j \tag{16}$$

In Eq. (12), $\overline{c_{i,jk}}$ is some average of $c_{i,j}$ and $c_{i,k}$, which also can be calculated for steady state. However, a simple arithmetic average, $\overline{c_{i,jk}} = (c_{i,j} + c_{i,k})/2$, was adopted because it provides good agreement with an analytical solution and a model with different cell-lengths (shown later). The harmonic mean in Eq. (12) is divided by 2, since b_j and b_k are calculated for x_j and x_k halved, while the concentration- and potential-gradients are calculated over the sum of the two halved distances. The Boltzmann factor, $g_{DL,i}$ in Eqs. (5) and (14), is divided by η_{rDL}, a factor to set the viscosity of the Donnan layer different from free pore water.

2.3. The electrical potential

Without external electrical field, $\Sigma z_i M_i = 0$, and $\psi_k - \psi_j$ can be solved from Eq. (12) [38]:

$$M_i = -D_i \frac{b_j b_k}{b_j + b_k} ((c_{i,k} - c_{i,j}) a_{i,k-j} + e_{i,k-j}) \tag{17}$$

where $e_{i,k-j}$ maintains electro-neutrality in the solutions:

$$e_{i,k-j} = z_i \overline{c_{i,jk}} \frac{\Sigma - D_i \frac{b_j b_k}{b_j + b_k} z_i (c_{i,k} - c_{i,j}) a_{i,k-j}}{\Sigma\, D_i \frac{b_j b_k}{b_j + b_k} z_i^2 \overline{c_{i,jk}}} \tag{18}$$

If an electrical potential field is applied, the resulting current comes partly from the chemical potential gradient and partly from the electric potential gradient:

$$I_{jk} = F \Sigma (z_i M_i)_{jk} = I_{d,jk} + I_{e,jk} \tag{19}$$

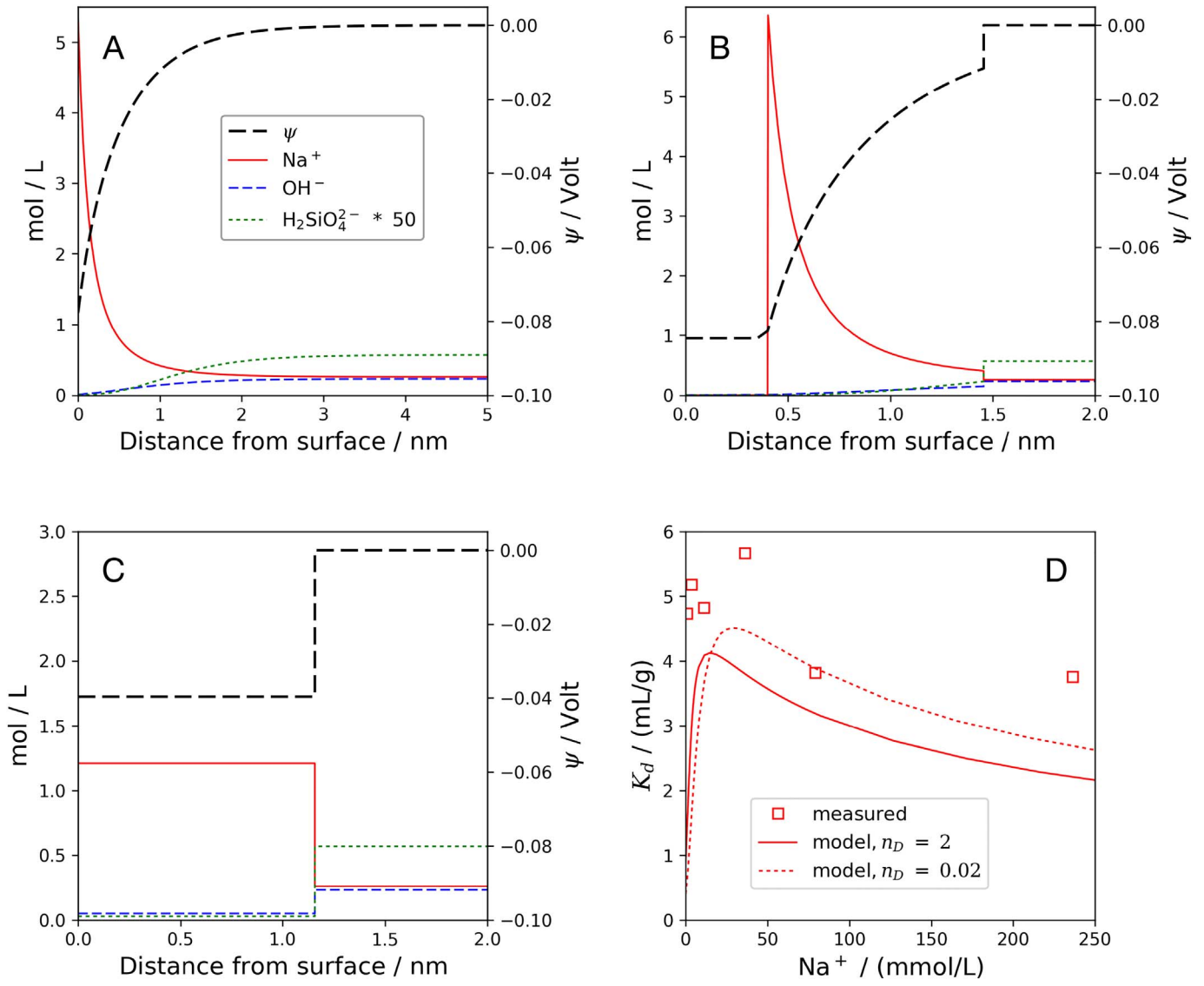

Fig. 3. Modeled concentrations and potential in the electrical double layer on the surface of $C_{0.85}SH$ as a function of distance, and the distribution coefficients of Na^+ in experiments of Hong and Glasser [31].
(A) Gouy-Chapman, going from the surface to where the potential is ≈ 0;
(B) with a limiting approach distance for the ions and integrating over 2 Debye lengths;
(C) the Donnan layer, also for 2 Debye lengths.
(D) The measured and modeled distribution coefficient of Na^+ in the experiments of Hong and Glasser, calculated with 2 and 0.02 Debye lengths.

where I_{jk} is the current from cell j to k (A) and subscripts d and e indicate the purely diffusive and the electrical component. It can be assumed that the current is equal for all cells (thus, no charge build-up in the cells, see [5]), which allows to calculate the potentials with Ohm's law. The resistance for electrical transport is:

$$R_{jk} = (\Delta\psi/n)/I_{e,jk} \tag{20}$$

where R_{jk} is the resistance (Ohm), $\Delta\psi$ is the electrical potential difference over the sample (V), and n is the number of cells. With the cells in series,

$$\sum_{j=0}^{n} I_{jk} R_{jk} = \Delta\psi \tag{21}$$

The equation can be solved for $I_{e,01}$ with Eq. (19) with the I_d values calculated by the model:

$$I_{e,01} \sum_{j=0}^{n} R_{jk} + \sum_{j=1}^{n} (I_{d,01} - I_{d,jk}) R_{jk} = \Delta\psi \tag{22}$$

With the potential ψ_0 given in boundary cell 0, the potential in the first cell becomes:

$$\psi_1 = \psi_0 + I_{e,01} R_{01} \tag{23}$$

With $I_{e,12} = I_{jk} - I_{d,12}$, the potential in the second cell is $\psi_2 = \psi_1 + I_{e,12} R_{12}$, and similarly for the other cells.

3. The individual contributions of ions to the current

The contribution of an ion to the specific conductance is [19,39]:

$$\Lambda_{m,i} = \frac{z_i^2 \mathrm{F}^2}{\mathrm{RT}} D_i \tag{24}$$

where $\Lambda_{m,i}$ is the molar conductivity [S / m / (mol/dm^3)]. The specific electrical conductance (SC) of the solution is the sum of the molar conductivity of the solutes multiplied with the concentration:

$$SC = \Sigma\,(\Lambda_{m,i}\, c_i) \tag{25}$$

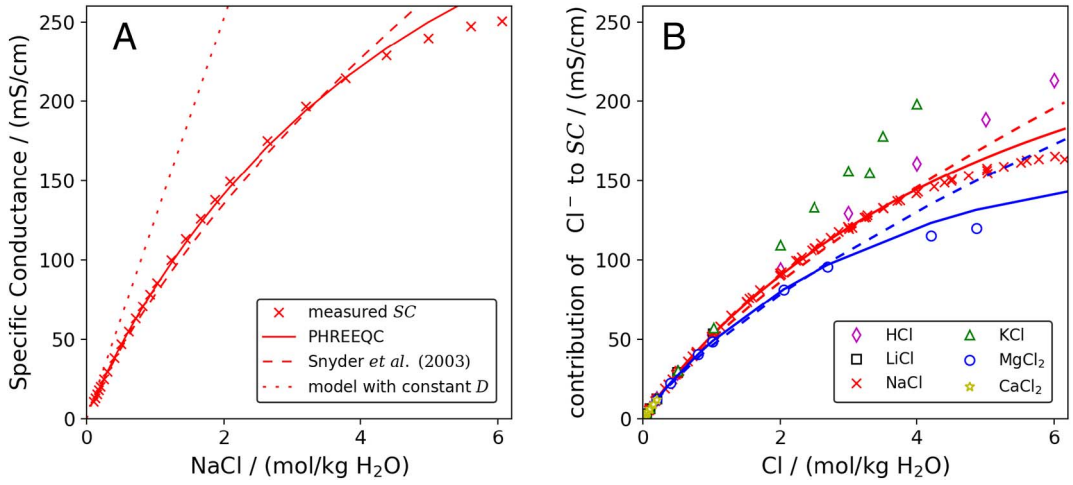

Fig. 4. (A) The measured specific conductance (*SC*) of NaCl solutions at 25 °C [42] and calculated with the models proposed here and by Snyder et al. [18], and with the diffusion coefficients of Na^+ and Cl^- fixed at their infinite-dilution values.
(B) The contribution of Cl^- to the *SC* of Cl-salt solutions at 25 °C calculated from transport numbers in HCl [43], LiCl [19], NaCl [19,44], KCl [19,44], $MgCl_2$ [45], $CaCl_2$ [46,47]. The full and dashed lines are from the model proposed in this paper and from [18], for NaCl and $MgCl_2$ in red and blue, respectively. (For interpretation of the references to color in this figure legend, the reader is referred to the web version of this article.)

It can be compared with the specific conductance from Ohm's law:

$$SC = 1/R = I/E, \tag{26}$$

where R is the resistance (m/S), I is the current density (Ampère/m^2), and E is the electric field (V/m).

The molar conductivities change with concentration and the composition of the solution. Fig. 4A shows the measured specific conductance of NaCl solutions as a function of concentration and calculated with the D_i's of Na^+ and Cl^- presumed constant at their infinite dilution value, and with the corrections proposed in this paper and by Snyder et al. [18]. It is evident that the constant-D model overestimates the conductance substantially, and increasingly with concentration. For molalities of 0.1 and 0.6, representative for the experiment in Fig. 1, the calculated *SC*'s are 1.2 and 1.4 too high, respectively. In addition, the presence of other salts affects the molar conductivity of the ions. Fig. 4B presents the contribution of Cl^- to the *SC* of binary solutions with H^+, alkalis, and alkaline earths. At concentrations < 1 M, the contribution is similar for the various salts, but at higher concentrations it diverges for different alkali-chloride salts and HCl, for the same Cl^- concentration. Normally, the differences can be attributed to complex formation of cations and anions, which reduces the conductance of the solution [19]. However, it is noted that Cl^- in NaCl solution is less conductive than in KCl solution, and it is doubtful that Na^+ forms a complex with Cl^- where the less hydrated K^+ does not. On the other hand, at concentrations above 1 M, the viscosity of NaCl increases much more rapidly than that of KCl, and the viscosity of the solution (rather than of pure water) could explain the differences in the overall *SC* that are difficult to model with the Onsager-Falkenhagen-Fuoss-MSA formulas [19,40,41]. However, Fig. 4B suggests that the relation between specific conductance and concentration may be more straightforward for concentrations smaller than 1 M.

3.1. Concentration and temperature dependence of the diffusion coefficients

As shown in Fig. 4, the one-parameter equation of Snyder et al. [18] gives quite good results for Na^+ and Cl^-, but there are deviations for other ions, and it is desirable to have the corrections available for more solutes. With two coefficients a_{1i} and a_{2i}, the diffusion coefficients can be made a function of the ionic strength I_s:

$$D_i = D^0_{T,i} \exp\left(\frac{-a_{1i} A\, |z_i|\, \sqrt{I_s}}{1 + \kappa a}\right) \tag{27}$$

where D^0_T is the diffusion coefficient at infinite dilution at T Kelvin, A is the Debye-Hückel A parameter (0.51 $(mol/dm^3)^{-0.5}$ at 25 °C), and κa is

$$\kappa a = \kappa \sqrt{I_s}\, \frac{a_{2i}}{1 + I_s^{0.75}} \qquad \kappa a = \left(10^{10} \times \kappa\right)^{-1} \frac{a_{2i}}{1 + I_s^{0.75}} \tag{28}$$

Eq. (27) follows Kohlrausch's law and similar relations reviewed in [39], except for the exponent that avoids negative D_i's, and the Debye-Hückel parameters that are present in all the theoretical equations [19,39,40].

The diffusion coefficients are corrected for temperature by a relation proposed by Smolyakov [41]:

$$D^0_{T,i} = D^0_{T=298,i} \frac{\eta^0_{298}\, T}{\eta^0_T\, 298.15} \exp\left(\frac{d_i}{T} - \frac{d_i}{298.15}\right) \tag{29}$$

where η^0_T is the viscosity of pure water (Pa·s) at T Kelvin and d_i is a coefficient. The exponential term dampens the temperature dependence of the diffusion coefficient, which is smaller than follows from the change of viscosity with temperature.

The coefficients a_{1i} and a_{2i} were optimized with the parameter optimization program PEST [48], first for Cl^- by using the transport numbers of NaCl solutions because the data for that salt are most complete and reliable [44]. For comparison, Table 3 gives the standard deviations of the calculated transport numbers of Cl^- in other solutions. With the numbers for Cl^- fixed, the coefficients a_{1i} and a_{2i} for other ions can be found from the conductance data at 25 and/or 20 °C referenced in Table 3. The coefficients a_{1i} and a_{2i} are assumed temperature independent. Values of d_i were obtained, first for Cl^- from $D^0_{Cl^-}$ values compiled by [49], and then for the other ions from the change of $\Lambda^0_{m,i}$ with temperature by using data from [19,50]. The coefficients are listed in Table 2. If undefined for a species, the suggested numbers are $d_i = 0$, $a_{1i} = 1.6$ and $a_{2i} = 4.73$, based on a set of *SC*'s of natural waters provided by Stuyfzand (pers. comm.).

Fig. 5 shows the correction factors for the diffusion coefficients of Na^+, K^+, OH^- and Cl^- as a function of the ionic strength, with the decreasing order for OH^-, Cl^- and Na^+ that follows the diffusion coefficient at infinite dilution according to Onsager theory [19]. K^+ is the exception, and it reveals the shortcoming of the correction method. The D^0 of K^+ is slightly smaller than that of Cl^-, and the K^+ line should lie below the Cl^- line. The viscosity of KCl solution is almost equal to the viscosity of pure water up to 2 M KCl, and the molar conductivities of both K^+ and Cl^- are almost independent of concentration up to 2 M KCl (*cf.* Fig. 4). Thus, when the K^+ conductivity is estimated from the

Table 2
Diffusion coefficients of selected solute species at 25 °C and infinite dilution, and coefficients for calculating their temperature- and ionic strength-dependence. Data sources, concentration ranges, and standard deviations of the model are given in Table 3.

Species	$D^0_{T=298}/10^{-9}$	d[a]	a_1[a]	a_2[a]
H^+	9.31	763	0.46	0
Na^+	1.33	122	1.52	3.7
K^+	1.96	395	2.5	21
NH_4^+	1.98	312	0.95	4.53
Mg^{2+}	0.705	111	2.4	13.7
Ca^{2+}	0.793	97	3.4	24.6
OH^-	5.27	553	0.52	0
Cl^-	2.03	194	1.6	6.9
SO_4^{2-}	1.07	34	2.08	13.4
$NaSO_4^-$	1.33	0	0.57	0
KSO_4^-	1.5	0	0	0
HCO_3^-	1.18	0	1.43	0
CO_3^{2-}	0.955	0	1.12	2.84
$NaCO_3^-$	1.2	0	0	0
NO_3^-	1.90	184	1.85	3.85

[a] a_1, a_2 and d in Eqs. (27), (28) and (29).

Table 3
Data of transport numbers of Cl^- and of molal conductance of salts, used for optimizing the coefficients in Table 2, and standard deviations of the fit.

Species	Salt	m[a] / (mol/L)	n[a]	$s.d.$ / %[a]	Data sources
Cl^-	NaCl[b]	0.01–6	23	0.9	[19,44]
	HCl	0.005–2	10	3.6	[43]
	KCl	0.001–0.5	9	2.9	[19,44]
	$MgCl_2$	0.2–3.7	11	2.9	[45]
	$CaCl_2$	0.0025–0.1	13	3.3	[46,47]
H^+	HCl	0.005–2	10	1.5	[51]
Na^+	NaCl	0.0001–4	47	1.3	[19,42,52]
K^+	KCl	0.1–1.3	22	1.1	[42,52]
NH_4^+	NH_4Cl	0.001–1	35	1.5	[50]
Mg^{2+}	$MgCl_2$	0.0001–2.1	21	2.4	[53]
Ca^{2+}	$CaCl_2$	0.0001–2	19	4.3	[19,50,54]
OH^-	NaOH	0.1–1.4	11	1.0	[55]
	KOH	0.09–1.2	13	1.4	[55]
SO_4^{2-}[c]	Na_2SO_4	0.02–1.7	23	0.7	[56]
	K_2SO_4	0.03–0.6	20	2.6	[55]
HCO_3^-[d]	$NaHCO_3$	0.06–0.8	12	3.0	[55]
	Na_2CO_3	0.05–1.7	12	9.3	[55]
	$KHCO_3$	0.05–1.3	11	6.0	[55]
	K_2CO_3	0.04–0.65	9	6.1	[55]
NO_3^-	$NaNO_3$	0.06–7.9	20	4.9	[55]
	KNO_3	0.05–1.3	11	5.4	[55]

[a] m = concentration range, n = number of samples, $s.d.$ / % = $100\sqrt{(1-\Lambda_{calc}/\Lambda_{obs})^2/(n-1)}$, where Λ is t_{Cl} for transport number calculations of Cl^-, or the sum of the molal conductances of cation and anion in the salt.
[b] For fitting a_1 and a_2 of Cl^-, NaCl is used; the $s.d.$ for other salts illustrates the deviations.
[c] Includes $NaSO_4^-$ and KSO_4^-.
[d] Includes CO_3^{2-} and $NaCO_3^-$.

conductivity of KCl solutions, it is increased to compensate for the smaller Cl^- conductivity that comes from the NaCl solutions.

4. Code validation

Krabbenhøft and Krabbenhøft [5] provided an analytical solution for the steady state of Friedmann's experiment shown in Fig. 1, that is compared with the numerical calculation in Fig. 6. The calculation is for the final stage of the experiment when the concentrations have stabilized after NaCl was added to the cathode reservoir. The two boundary solutions contain 25 mM NaOH and 83 mM KOH, with 500 mM NaCl extra in the cathode cell, and the imposed electric field is 3 V on a 10 mm column.

The numerical model gives an excellent agreement with the analytical solution when the cells are refined at the column ends where the concentrations change abruptly with distance. The results shown in Fig. 6 were obtained with 10 cells of 0.1 mm length at the ends, and 5 cells of 1.6 mm in the middle, thus, 25 cells for the 10 mm sample. It is of interest to note that in most of the column, the ratios of the concentrations are determined by the ratios in the source reservoir, thus, the anode reservoir for the cations (K / Na = 83 / 25 = 3.32), and the cathode reservoir for the anions (Cl / OH = 500 / 108 = 4.63). For example, in the middle of the column, at 5 mm, K / Na = 275 / 82.9 (= 3.32), and Cl / OH = 294.4 / 63.6 (= 4.63). The ratios follow from the constant fluxes and the time-invariant concentrations for an ion at each point in the column in the steady state.

5. Application

It was noted that the measured current requires a smaller geometrical factor than the one for calculating the Cl^- breakthrough in Friedmann's experiment in Fig. 1. Can a pore with a Donnan layer explain the discrepancy?

With $dc_i / dx = 0$, the current density is:

$$I = -\frac{F^2}{RT}\frac{\varepsilon}{G}\sum z_i^2 D_i c_i \frac{d\psi}{dx} \tag{30}$$

In the Donnan pore, the concentrations are (Eqs. (5) and (8)):

$$c_i = f_{free}c_{free,i} + (1-f_{free})c_{DL,i} = c_{free,i}(f_{free} + (1-f_{free})g_{DL,i}) \tag{31}$$

According to the Boltzmann Eq. (5), the g_{DL}'s invert for oppositely charged ions with the same charge number. Then, with only single-charged ions in solution, Eq. (4) results in a quadratic equation that can be solved for $g_{DL,i}$:

$$g_{DL,i}^2 + \frac{Su}{\nu_{DL}\sum c_i/2}g_{DL,i} - 1 = 0 \tag{32}$$

Furthermore, ν_{DL} and f_{free} can be found for a number of Debye lengths (n_D) for the thickness of the Donnan layer, and with the pore radius estimated from:

$$r = 2V_{pore}/A_{pore} = 2\,V_1\,\varepsilon_c/(A_c \times \rho_c) \tag{33}$$

where V_1 is the volume of 1 cm^3 cement with the associated water and aggregate ($= 1 + \rho_c \times w/c + \rho_c / \rho_s \times s/c$), ε_c is the capillary porosity, A_c is the specific surface of the cement minerals (assumed 100 m^2/(g c)), and ρ_c and ρ_s are the densities of the cement and aggregate (3.2 and 2.6 g/cm^3, respectively). The surface area of the aggregate is neglected.

Taken together, the fraction of free pore water is:

$$f_{free} = \frac{(r - n_D/\kappa)^2}{r^2} \tag{34}$$

Thus, for the first 44 h of Friedmann's experiment, the current can be calculated as a function of the surface charge with the parameters given in Table 4, where $\varepsilon / G = 0.0116$ [5]. The result is plotted in Fig. 7A with $n_D = 2$ and 4. First, it can be noted that the current is smaller than in Fig. 1 when the surface charge is zero, because the diffusion coefficients are lower when they are corrected for the ionic strength of the solution. Second, less surface charge is needed to obtain a current density of 11 A/m^2 when the charge is positive instead of negative. The reason is that OH^-, with the highest diffusion coefficient of the ions that are present, increases in concentration in the Donnan layer of a positive surface and gets a higher overall concentration in the pore water. Third, when the negative surface is small, the current is smaller than without surface charge. This is because OH^- is rejected from the surface and thus has a lower overall concentration in the pore. When the surface turns more negative, the higher concentration of cations in the Donnan layer compensates the loss of OH^- and lets the current increase. Finally, increasing the size of the Donnan layer, equivalent to decreasing f_{free}, lowers the current. This follows from taking the derivative of Eq. (31) with respect to f_{free} for both cations and

Table 4
The electro-chemical properties of a Donnan pore in Friedmann's experiment in a 33.18 mL column with $w/c = 0.7$ and $s/c = 0.333$. The concentrations are for $t = 0$ and for $t = 44$ h, when 0.5 M NaCl was added to the cathode reservoir.

V_1[a]	ε_c[b]	r[c]	I_s[d]	f_{free}	Su[e]	*Ion*	D[f]	c_{free}[g]	g_{DL}	c[g]	G[h]	I[i]
3.65	0.309	7.06	0.108	0.54	21.1	Na^+	1.10	25	0.56	20	26.7	11.0
						K^+	1.70	83	0.56	66		
						OH^-	4.83	108	1.78	135		
After adding 0.5 M NaCl:												
			0.608	0.79	21.1	Na^+	0.90	525	0.79	502	26.7	24.2
						K^+	1.54	83	0.79	79		
						OH^-	4.29	108	1.26	113		
						Cl^-	1.49	500	1.26	523		

[a] Volume of 1 cm^3 cement with water and aggregate ($= 1 + \rho_c \times w/c + \rho_c / \rho_s \times s/c$, cm^3).
[b] Capillary porosity from Powers' equation ($\rho_c \times w/c - f_e \times \alpha_t$) / V_1, $f_e = 1.15$ [57] and $\alpha_t = 0.239 + 0.745 \times \tanh(3.62 \times (w/c - 0.095))$ [17].
[c] Pore radius (nm).
[d] Ionic strength (mol/L).
[e] Surface charge (μeq/g cement), *Su* in Eq. (32) divided by g cement in the column.
[f] Diffusion coefficient at 25 °C, corrected for ionic strength ($m^2/s / 10^{-9}$).
[g] Average concentration in pore water (mol/m^3 water).
[h] Geometrical factor (−) for $\varepsilon_c / G = 0.0116$ [5].
[i] Ampère/m^2 with $d\psi / dx = 300$ V/m.

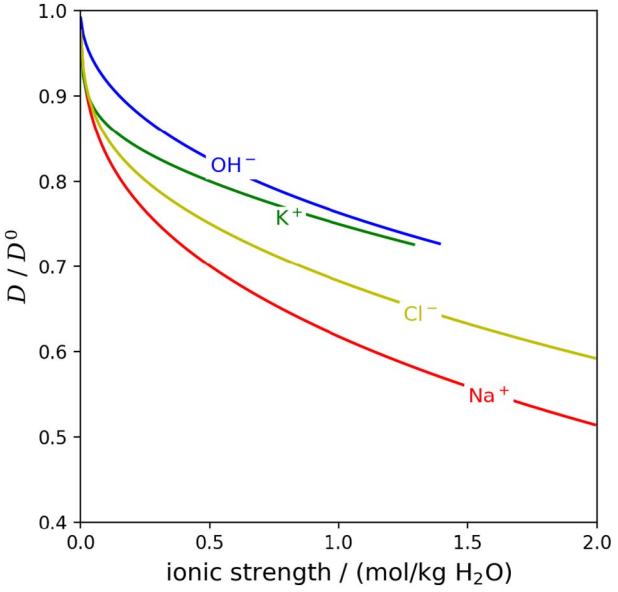

Fig. 5. The correction factor for the ionic strength dependence of the (electro-)diffusion coefficient of Na^+, K^+, OH^- and Cl^-.

anions, which is always positive if only single-charged ions are present.

A surface charge of 0 and the surface charges that give a current density of 11 A/m^2 were introduced in the numerical model, and the results are shown in Fig. 7B. In all three cases, the model correctly gives the initial current that is calculated by hand. But when NaCl is added the curves diverge considerably, and the trends can be related to the model properties. With a negative surface charge in the model, the diffusion of Na^+ is enhanced and the current rises quickly and to a far higher level than measured when Cl^- has arrived at the anode end (dotted line in Fig. 7B). When a positive surface charge is added, the diffusion of Na^+ is reduced so that the current levels off to a (pseudo-) steady state below the measured current. Without surface charge, the initial current is too small, and the increase rate is too high.

If the Cl^- curves in Fig. 7B and Fig. 1 are compared, it can be seen that the correction of the diffusion coefficient brings the models with a zero or positive surface charge closer to the observed mole transfer. A negative surface reduces the accessible porosity for Cl^- and lets Cl^- arrive too early. Thus, a negative surface is inappropriate for modeling electro-migration in this experiment. As regards the zero surface charge, it is possible to fit the initial current by decreasing the geometrical factor, and counter the concomitant faster arrival of Cl^- by introducing sorption, but it is simply impossible to deal with the consequence that the current increase rate then will go far beyond what is

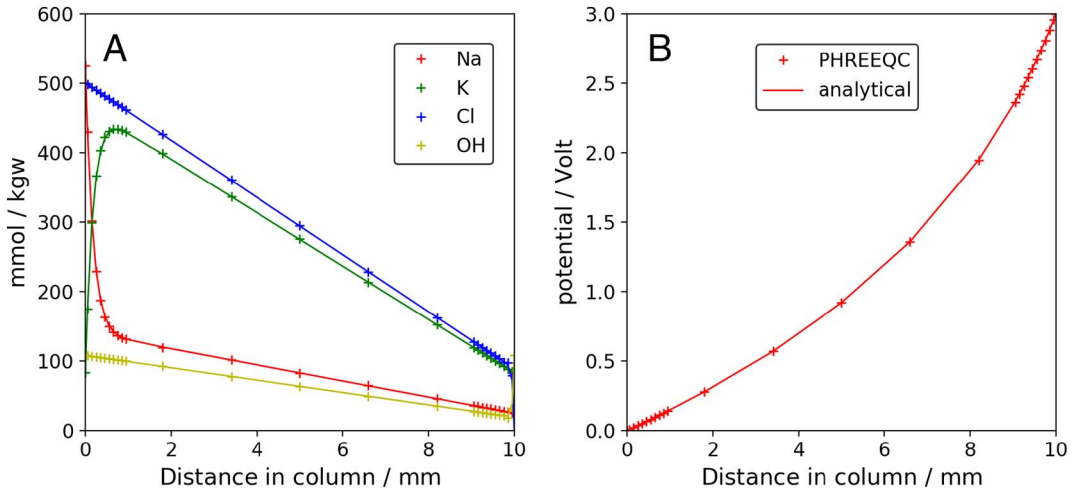

Fig. 6. (A) Steady state concentrations of Na^+-, K^+-, Cl^-- and OH^--concentrations with distance in Friedmann's experiment. (B) The steady state potential over the sample. In (A) and (B), lines from the analytical solution, + symbols from the numerical model.

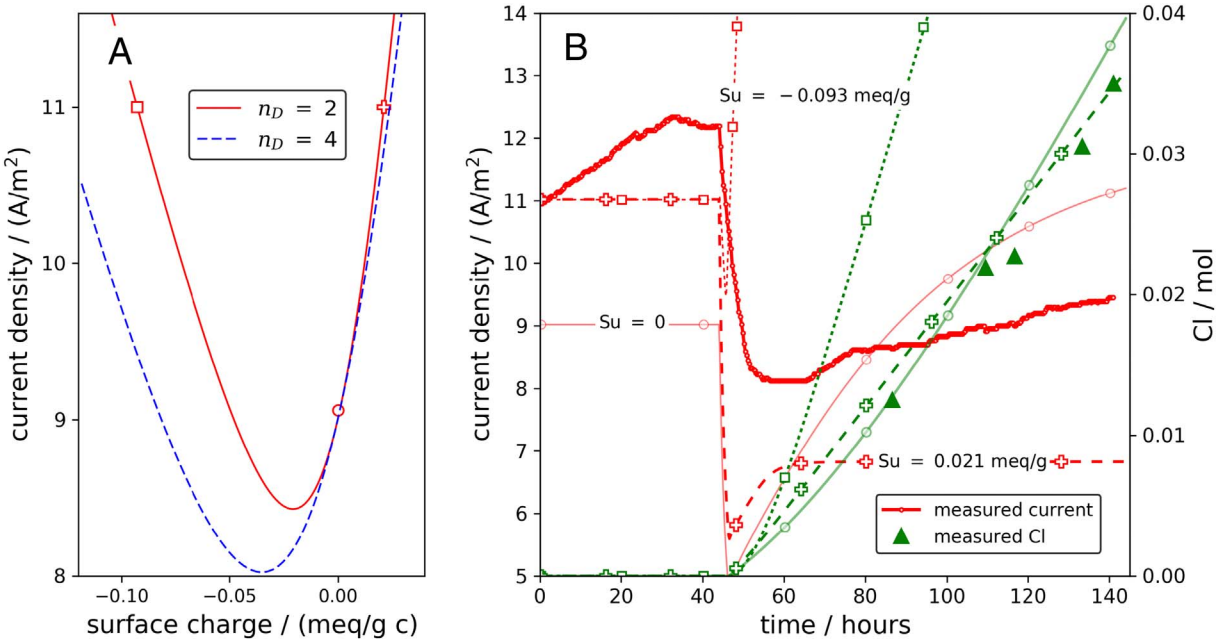

Fig. 7. (A) The current density in Friedmann's experiment as a function of the surface charge, with a Donnan layer that has a thickness of 2 or 4 Debye lengths, calculated with the concentrations and electro-migration parameters of the initial conditions in Table 4. Markers indicate the surface charges used in the model calculations in (B).
(B) Current density and Cl^- calculated for Friedmann's experiment with PHREEQC, with surface charges 'Su' of 0, −0.093, or 0.021 meq/g cement and n_D = 2. The concentrations are given in Tables 4, and 0.5 M NaCl is added to the cathode reservoir after 44 h. The calculations were done with the modified database phreeqc.dat that contains the concentration- and temperature dependence of the species' diffusion coefficients from Table 2.

measured.

The current from the model with a positive surface is also not satisfying yet. It does not match with the current increase that starts when the electrical field is applied, it increases sharply instead of gradually when Cl^- breaks through, and after that, it remains below the measured current. However, the discrepancies are manageable; they can be related to kinetic chemical reactions of cement minerals and to exchange of water in mobile and immobile zones as will be shown in more complete model calculations in another paper.

6. Discussion

The proposed model has a bipartite division of the pore space with a charged part in a Donnan layer (DL) on the surfaces lining the pore, and an uncharged part of 'free' pore water. In the DL, the surface charge is compensated by an increase of counter-ions and a decrease of co-ions relative to the free pore water. It allows calculating the diffusion of ions and the current in electro-migration experiments easily, but the question is how well it applies to the complicated pore space in a concrete. Purely computationally, the average concentrations in the DL of a mixture of ions, with different charge numbers, agree well with what is calculated by a full, numerical integration of the Gouy-Chapman equation of the electrical double layer [30]. If the average concentrations in the pore are the same, the Nernst-Planck equation will give the same results for the flux, irrespective of a further subdivision of the double layer. However, it is likely that the higher concentrations close to the surface go hand-in-hand with changing transport properties of the ions, probably decreasing the diffusion coefficient. Perhaps these changes in transport properties can be accounted for by modifying the diffusion coefficients as a function of the ionic strength. Alternatively, in PHREEQC the viscosity of the DL can be changed relative to free water (thus affecting all the solutes in the DL in equal manner), or individual ions can be given an enrichment factor in the DL. The options may be helpful for modeling detailed experiments, but perhaps they are unnecessary, since diffusion experiments in clays have shown that the two-fold division of the pore without these corrections, already gives a good approximation of the accessible porosity of ions ($c / c_{free} \times \varepsilon$) and the pore water diffusion coefficient ($D_p = D / G$) [37,58,59].

It is often assumed in transport models that all the solutes have the same ε / G factor in porous media although there is abundant experimental evidence from studies with clay minerals and –rocks that the reality is different [37,58–63], and the DL model offers an approach for generalizing the variation. The ratio c / c_{free} gives the difference that otherwise is attributed to another ε / G, and the ratios change when the solution compositions change in transient conditions.

From the combination of measured current and effective diffusion coefficient of Cl^- ($D_e = D \times \varepsilon / G$), the DL model can calculate the overall surface charge of the minerals that line the pores. In the experiment that lies at the heart of this paper, the surface charge is positive, and estimated at +21 μeq/g c. In a rough calculation, the charge can be linked with the minerals in the column. From the chemical analysis in [4], the cement has 41% CSH, which, with the surface complexation model of [28] and the pore water in equilibrium with portlandite, gives a charge of −6.8 μeq/g c. If all the positive charge is attributed to 6% AFm, it is +0.456 meq/g, which is possible given its structure [27]. For comparison, the charge of the clay mineral smectite is −0.8 meq/g [36, p. 251].

Two more model aspects in this paper differ from other models for electro-migration experiments [2,5,64–66]. The diffusion coefficients of the individual ions are corrected for ionic strength of the solution in accordance with measured transport numbers and solution conductivities. This correction is done apart from the activity coefficient correction (γ) for the driving force ($\partial c / \partial x$) in the Nernst-Planck equation. Thus, if ($\partial c / \partial x$) is assumed zero, the calculated current is still affected by the ionic strength: the current is smaller for Friedmann's experiment than when the D's of zero ionic strength are used. Both the γ and the D correction depend on the electrostatic properties of the solution, so both correction terms contain Debye-Hückel parameters. The D correction applies well for ionic strengths $\sim <$ 1 M and for NaCl solutions up to 4 M, and results in the following corrections: D / D^0 = 0.83, 0.89 and 0.92 for Na^+, K^+ and OH^-, respectively, at ionic strength of 0.11 (Table 4). Clearly, Nernst-Planck models must use the diffusion coefficients that conform to reality. Furthermore, when diffusivities are compared in models for the concrete pore structure

[3,67], the measured effective diffusion coefficient should be related to the free water diffusion coefficient at the ionic strength of the solution, but the relation is complicated if the surface charge is not accounted for in the model.

The other aspect is that Ohm's law is used for calculating the electrical potential gradient, where other models invoke Poisson's law, $d^2\psi / dx^2 = -F \Sigma zc / \varepsilon_w$ [2,5,64,66]. However, the precision of PHREEQC (and in fact, of any numerical model for calculating chemical reactions) is not better than about 10^{-8} mol/m^3, implying that $d^2\psi / dx^2$ that is calculated from charge imbalance cannot be more precise than 1.4×10^6 V/m^2. This is twice higher than the maximum in the various stages of Friedmann's experiment, and insufficient for calculating the potential. Samson et al. [6] also noted problems with the numerical model that uses Poisson's law. However, the charge from Poisson's law is so small [5] that it can be neglected and then, Ohm's law is a viable alternative.

7. Conclusions

- The division of pore water into a charged Donnan-layer part and an uncharged, 'free' part facilitates the calculation of ion transport in the charged pores of concrete with the Nernst-Planck equation.
- The charge in the Donnan layer counterbalances the charge of concrete mineral surfaces that line the pores. Electro-migration experiments in which both the current and the Cl^- breakthrough are measured following the addition of NaCl to the cathode reservoir, allow estimating the surface charge of the minerals in a concrete pore. It is positive in Friedmann's experiment [4], where it enhances diffusion of anions and reduces diffusion of cations.
- In calculations with the Nernst-Planck equation, the diffusion coefficients of individual ions must be corrected for ionic strength of the solution. This correction also affects the transport numbers of the individual ions. The proposed correction is generally accurate up to ~1 M, and up to 4 M for NaCl.
- When the diffusivity (the ratio of the porosity and the geometrical factor) is calculated from experiments, the reference is the diffusion coefficient at the ionic strength of the solution, not the one at infinite dilution. The diffusivities are different for different cations and anions, and a function of the ionic strength, the pore radius and the surface charge of the minerals.
- The comparison of experimental and model results suggests a role for kinetic portlandite dissolution and mobile/immobile water exchange.
- The full Nernst-Planck equation has been programmed in PHREEQC, which now can calculate the current in electro-migration experiments, or the electrical potential in diffusion experiments without an external electrical field. Input files for calculating Figs. 1 and 3–7 are listed in the Appendix A and are available for downloading.

Acknowledgements

I like to thank Pierre Henocq, who asked for inclusion of the full Nernst-Planck equation in PHREEQC; David Parkhurst for invaluable support in checking the code and for commenting on a draft of this paper; ANDRA for financial support, contract 064069STR; two reviewers whose comments have been addressed in the paper.

Appendix A

Website http://www.hydrochemistry.eu/pub/el_dif/concrete1.zip contains files for calculating Figs. 1 and 3–7, and the composition of the concrete used by Friedmann with Tennis and Jennings' model. Extract the files, and keep them together in a directory since experimental data are plotted from files that are expected to be in the same directory as the PHREEQC file. The PHREEQC files should be run with phreeqc.exe from http://www.hydrochemistry.eu/ph3/index.html.

The files are:

Fig1.phr: calculates and plots the Friedmann experiment with parameters from Krabbenhøft and Krabbenhøft, and from Narsilio et al.

Fig3a-b.zip: Matlab files that integrate the Gouy-Chapman double layer.

Fig3d.phr: calculates the distribution coefficient of Na^+.

Fig4a.phr: calculates and plots the specific conductance (*SC*) of NaCl solutions.

Fig4b.phr: calculates and plots the contribution of Cl^- to the *SC* of various salts.

Fig5.py: python file that plots the ionic strength dependence of D_i's of solute species.

Fig6.phr: calculates and plots the steady state analytical solution of Krabbenhøft and Krabbenhøft.

Fig7a.phr: calculates and plots the current density as a function of the surface charge.

Fig7b.phr: calculates and plots Friedmann's experiment with three different surface charges.

Tennis.phr: calculates and plots (Figs. A1 and A2) the composition of Friedmann's concrete as a function of the aluminate hydration with the model of Tennis and Jennings, 2000, CCR 30, 855.

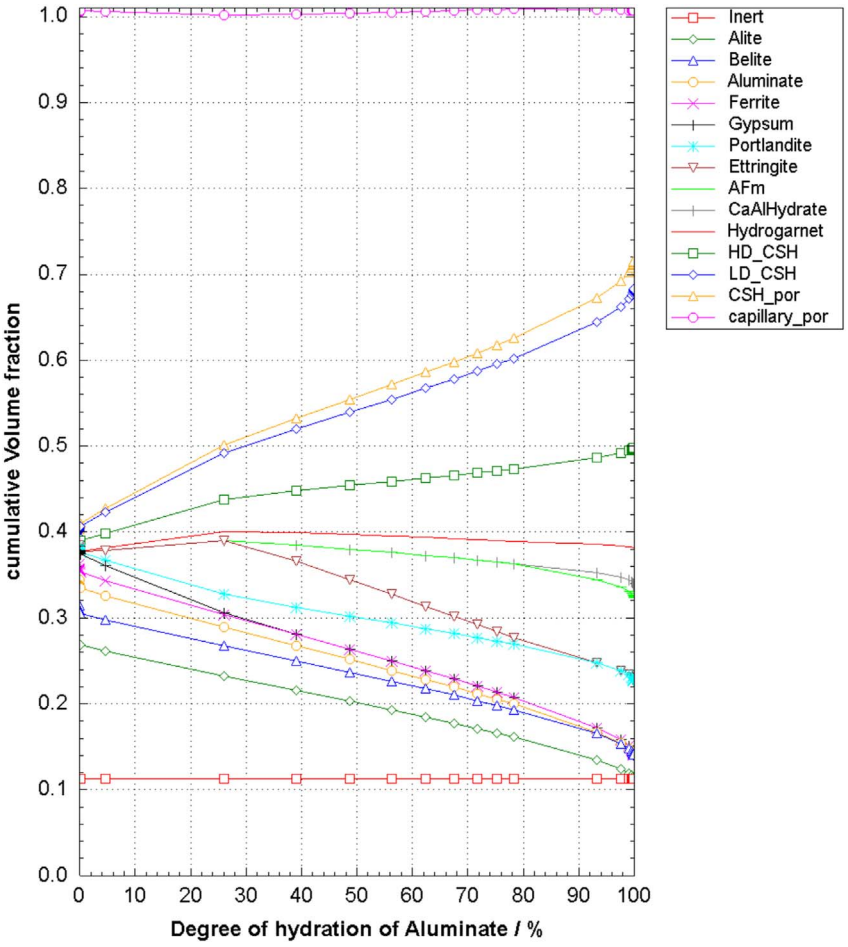

Fig. A1. The volume fractions of the components in Friedmann's concrete with $w/c = 0.7$ as a function of the aluminate hydration.

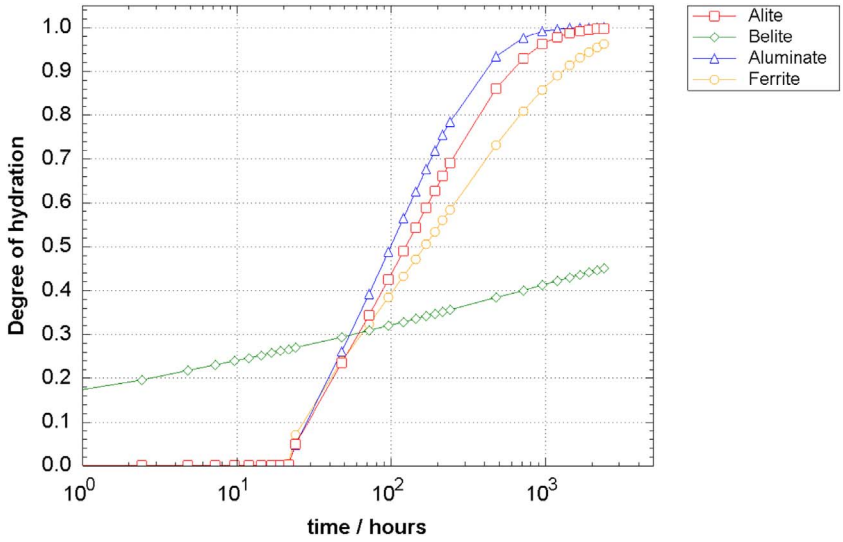

Fig. A2. The degree of hydration of the clinker minerals in Friedmann's experiment.

References

[1] C. Andrade, Calculation of chloride diffusion coefficients in concrete from ionic migration measurements, Cem. Concr. Res. 23 (1993) 724–742.
[2] G.A. Narsilio, R. Li, P. Pivonka, D.W. Smith, Comparative study of methods used to estimate ionic diffusion coefficients using migration tests, Cem. Concr. Res. 37 (2007) 1152–1163.
[3] R.A. Patel, Q.T. Phung, S.C. Seetharam, J. Perko, D. Jacques, N. Maes, G. De Schutter, G. Ye, K. Van Breugel, Diffusivity of saturated ordinary Portland cement-based materials: a critical review of experimental and analytical modelling approaches, Cem. Concr. Res. 90 (2016) 52–72.
[4] H. Friedmann, O. Amiri, A. Aıt-Mokhtar, P. Dumargue, A direct method for determining chloride diffusion coefficient by using migration test, Cem. Concr. Res. 34 (2004) 1967–1973.
[5] K. Krabbenhøft, J. Krabbenhøft, Application of the Poisson–Nernst–Planck equations to the migration test, Cem. Concr. Res. 38 (2008) 77–88.
[6] E. Samson, J. Marchand, K.A. Snyder, Calculation of ionic diffusion coefficients on

the basis of migration test results, Mater. Struct. 36 (2003) 156–165.
[7] C.C. Yang, S.C. Chiang, L.C. Wang, Estimation of the chloride diffusion from migration test using electrical current, Constr. Build. Mater. 21 (2007) 1560–1567.
[8] E. Samson, J. Marchand, Modeling the effect of temperature on ionic transport in cementitious materials, Cem. Concr. Res. 37 (2007) 455–468.
[9] Y. Elakneswaran, T. Nawa, K. Kurumisawa, Electrokinetic potential of hydrated cement in relation to adsorption of chlorides, Cem. Concr. Res. 39 (2009) 340–344.
[10] M.V.A. Florea, H.J.H. Brouwers, Chloride binding related to hydration products: part I: ordinary Portland cement, Cem. Concr. Res. 42 (2012) 282–290.
[11] E.J. Garboczi, D.P. Bentz, Computer simulation of the diffusivity of cement-based materials, J. Mater. Sci. 27 (1992) 2083–2092.
[12] P. Halamickova, R.J. Detwiler, D.P. Bentz, E.J. Garboczi, Water permeability and chloride ion diffusion in Portland cement mortars: relationship to sand content and critical pore diameter, Cem. Concr. Res. 25 (1995) 790–802.
[13] J.D. Shane, T.O. Mason, H.M. Jennings, E.J. Garboczi, D.P. Bentz, Effect of the interfacial transition zone on the conductivity of Portland cement mortars, J. Am. Ceram. Soc. 83 (2000) 1137–1144.
[14] A. Delagrave, J. Marchand, M. Pigeon, Influence of microstructure on the tritiated water diffusivity of mortars, Adv. Cem. Based Mater. 7 (1998) 60–65.
[15] S. Kamali-Bernard, F. Bernard, W. Prince, Computer modelling of tritiated water diffusion test for cement based materials, Comput. Mater. Sci. 45 (2009) 528–535.
[16] M. Zhang, G. Ye, K. Van Breugel, Microstructure-based modeling of water diffusivity in cement paste, Constr. Build. Mater. 25 (2011) 2046–2052.
[17] S. Bejaoui, B. Bary, Modeling of the link between microstructure and effective diffusivity of cement pastes using a simplified composite model, Cem. Concr. Res. 37 (2007) 469–480.
[18] K.A. Snyder, X. Feng, B.D. Keen, T.O. Mason, Estimating the electrical conductivity of cement paste pore solutions from OH^-, K^+ and Na^+ concentrations, Cem. Concr. Res. 33 (2003) 793–798.
[19] R.A. Robinson, R.H. Stokes, Electrolyte Solutions: The Measurement and Interpretation of Conductance, Chemical Potential, and Diffusion in Solutions of Simple Electrolytes, Butterworths Scientific Publications, London, 1959.
[20] L. Tong, O.E. Gjørv, Chloride diffusivity based on migration testing, Cem. Concr. Res. 31 (2001) 973–982.
[21] C.C. Yang, S.W. Cho, R. Huang, The relationship between charge passed and the chloride-ion concentration in concrete using steady-state chloride migration test, Cem. Concr. Res. 32 (2002) 217–222.
[22] S. Galı, C. Ayora, P. Alfonso, E. Tauler, M. Labrador, Kinetics of dolomite–portlandite reaction: application to Portland cement concrete, Cem. Concr. Res. 31 (2001) 933–939.
[23] D. Planel, J. Sercombe, P. Le Bescop, F. Adenot, J.-M. Torrenti, Long-term performance of cement paste during combined calcium leaching–sulfate attack: kinetics and size effect, Cem. Concr. Res. 36 (2006) 137–143.
[24] N.C. Marty, F. Claret, A. Lassin, J. Tremosa, P. Blanc, B. Madé, E. Giffaut, B. Cochepin, C. Tournassat, A database of dissolution and precipitation rates for clay-rocks minerals, Appl. Geochem. 55 (2015) 108–118.
[25] H. Friedmann, O. Amiri, A. Aït-Mokhtar, Physical modeling of the electrical double layer effects on multispecies ions transport in cement-based materials, Cem. Concr. Res. 38 (2008) 1394–1400.
[26] U.A. Birnin-Yauri, F.P. Glasser, Friedel's salt, $Ca_2Al(OH)6(Cl, OH)\cdot 2H_2O$: its solid solutions and their role in chloride binding, Cem. Concr. Res. 28 (1998) 1713–1723.
[27] T. Runčevski, R.E. Dinnebier, O.V. Magdysyuk, H. Pöllmann, Crystal structures of calcium hemicarboaluminate and carbonated calcium hemicarboaluminate from synchrotron powder diffraction data, Acta Crystallogr. Sect. B: Struct. Sci. 68 (2012) 493–500.
[28] H. Viallis-Terrisse, A. Nonat, J.-C. Petit, Zeta-potential study of calcium silicate hydrates interacting with alkaline cations, J. Colloid Interface Sci. 244 (2001) 58–65.
[29] D.L. Parkhurst, C.A.J. Appelo, Description of input and examples for PHREEQC version 3—a computer program for speciation, batch-reaction, one-dimensional transport, and inverse geochemical calculations, US Geol. Surv. Tech. Methods Book, 6 2013, p. 497.
[30] C.A.J. Appelo, P. Wersin, Multicomponent diffusion modeling in clay systems with application to the diffusion of tritium, iodide, and sodium in opalinus clay, Environ. Sci. Technol. 41 (2007) 5002–5007.
[31] S.-Y. Hong, F.P. Glasser, Alkali binding in cement pastes: part I. The CSH phase, Cem. Concr. Res. 29 (1999) 1893–1903.
[32] J. Haas, Etude expérimentale et modélisation thermodynamique du système CaO-SiO_2-(Al_2O_3)-H_2O, Université de Bourgogne, 2012.
[33] J. Haas, A. Nonat, From C–S–H to C–A–S–H: experimental study and thermodynamic modelling, Cem. Concr. Res. 68 (2015) 124–138.
[34] B. Lothenbach, A. Nonat, Calcium silicate hydrates: solid and liquid phase composition, Cem. Concr. Res. 78 (2015) 57–70.
[35] B. Lothenbach, T. Matschei, G. Möschner, F.P. Glasser, Thermodynamic modelling of the effect of temperature on the hydration and porosity of Portland cement, Cem. Concr. Res. 38 (2008) 1–18.
[36] C.A.J. Appelo, D. Postma, Geochemistry, Groundwater and Pollution, CRC press, 2005.
[37] C. Tournassat, C.A.J. Appelo, Modelling approaches for anion-exclusion in compacted Na-bentonite, Geochim. Cosmochim. Acta 75 (2011) 3698–3710.
[38] J.R. Vinograd, J.W. McBain, Diffusion of electrolytes and of the ions in their mixtures, J. Am. Chem. Soc. 63 (1941) 2008–2015.
[39] H. Harned, B. Owen, The Physical Chemistry of Electrolyte Solutions, 3rd ed, Reinhold, N. Y, 1958.
[40] J.-C. Justice, J. Périé, M. Périé, Ionic interactions in solutions. V. Transference number variation with concentration—contribution to a theoretical interpretation for binary symmetrical electrolytes, J. Solut. Chem. 9 (1980) 583–605.
[41] A. Anderko, M.M. Lencka, Computation of electrical conductivity of multicomponent aqueous systems in wide concentration and temperature ranges, Ind. Eng. Chem. Res. 36 (1997) 1932–1943.
[42] J.F. Chambers, J.M. Stokes, R.H. Stokes, Conductances of concentrated aqueous sodium and potassium chloride solutions at 25, J. Phys. Chem. 60 (1956) 985–986.
[43] A. Davies, B. Steel, Transference numbers for ultra concentrated solutions of aqueous hydrochloric acid at 25 °C, J. Solut. Chem. 13 (1984) 349–356.
[44] D.K. Panopoulos, H. Kaneko, M. Spiro, Transference numbers of sodium chloride in concentrated aqueous solutions and chloride conductances in several concentrated electrolyte solutions, J. Solut. Chem. 15 (1986) 243–252.
[45] H. Schönert, Transference numbers in the H_2O + NaCl + $MgCl_2$ system at T = 298.15 K, determined in a five-compartment Hittorf cell, J. Solut. Chem. 43 (2014) 26–39.
[46] T. Shedlovsky, D.A. MacInnes, The determination of activity coefficients from the potentials of concentration cells with transference. III. Potassium chloride. IV. Calcium chloride, J. Am. Chem. Soc. 59 (1937) 503–506.
[47] A.G. Keenan, H.G. McLeod, A.R. Gordon, The variation of the transference numbers for calcium chloride in aqueous solution with temperature. III, J. Chem. Phys. 13 (1945) 466–469.
[48] J. Doherty, PEST, Model-independent Parameter Estimation: User Manual, 5th edn, Addendum to the PEST Manual, Watermark, Brisb. Aust, 2015 Available at http://www.pesthomepage.org.
[49] R. Mills, V.M. Lobo, Self-Diffusion in Electrolyte Solutions: A Critical Examination of Data Compiled From the Literature, Elsevier, 1989.
[50] R.B. McCleskey, Electrical conductivity of electrolytes found in natural waters from (5 to 90) °C, J. Chem. Eng. Data 56 (2011) 317–327.
[51] W.J. Hamer, H.J. DeWane, Electrolytic Conductance and the Conductances of Halogenic Acids in Water, Nat. Stand. Ref. Data Ser., Nat. Bur. Stand. (U.S.), 1970.
[52] Y.-F. Hu, X.-M. Zhang, J.-G. Li, Q.-Q. Liang, Semi-ideal solution theory. 2. Extension to conductivity of mixed electrolyte solutions, J. Phys. Chem. B 112 (2008) 15376–15381.
[53] D.G. Miller, J.A. Rard, L.B. Eppstein, J.G. Albright, Mutual diffusion coefficients and ionic transport coefficients lij of magnesium chloride-water at 25 °C, J. Phys. Chem. 88 (1984) 5739–5748.
[54] T. Isono, Density, viscosity, and electrolytic conductivity of concentrated aqueous electrolyte solutions at several temperatures. Alkaline-earth chlorides, lanthanum chloride, sodium chloride, sodium nitrate, sodium bromide, potassium nitrate, potassium bromide, and cadmium nitrate, J. Chem. Eng. Data 29 (1984) 45–52.
[55] W.M. Haynes, CRC Handbook of Chemistry and Physics, CRC Press, 2014.
[56] R. Buchner, S.G. Capewell, G. Hefter, P.M. May, Ion-pair and solvent relaxation processes in aqueous Na_2SO_4 solutions, J. Phys. Chem. B 103 (1999) 1185–1192.
[57] D.P. Bentz, Influence of water-to-cement ratio on hydration kinetics: simple models based on spatial considerations, Cem. Concr. Res. 36 (2006) 238–244.
[58] C.A.J. Appelo, L.R. Van Loon, P. Wersin, Multicomponent diffusion of a suite of tracers (HTO, Cl, Br, I, Na, Sr, Cs) in a single sample of Opalinus clay, Geochim. Cosmochim. Acta 74 (2010) 1201–1219.
[59] M.A. Glaus, M. Aertsens, C.A.J. Appelo, T. Kupcik, N. Maes, L. Van Laer, L.R. Van Loon, Cation diffusion in the electrical double layer enhances the mass transfer rates for Sr^{2+}, Co^{2+} and Zn^{2+} in compacted illite, Geochim. Cosmochim. Acta 165 (2015) 376–388.
[60] L.R. Van Loon, J.M. Soler, A. Jakob, M.H. Bradbury, Effect of confining pressure on the diffusion of HTO, $^{36}Cl^-$ and $^{125}I^-$ in a layered argillaceous rock (Opalinus clay): diffusion perpendicular to the fabric, Appl. Geochem. 18 (2003) 1653–1662.
[61] L.R. Van Loon, M.A. Glaus, W. Müller, Anion exclusion effects in compacted bentonites: towards a better understanding of anion diffusion, Appl. Geochem. 22 (2007) 2536–2552.
[62] M.A. Glaus, S. Frick, R. Rossé, L.R.Van Loon, Comparative study of tracer diffusion of HTO, $^{22}Na^+$ and $^{36}Cl^-$ in compacted kaolinite, illite and montmorillonite, Geochim. Cosmochim. Acta 74 (2010) 1999–2010.
[63] C.A.J. Appelo, A. Vinsot, S. Mettler, S. Wechner, Obtaining the porewater composition of a clay rock by modeling the in- and out-diffusion of anions and cations from an in-situ experiment, J. Contam. Hydrol. 101 (2008) 67–76.
[64] E. Samson, J. Marchand, Numerical solution of the extended Nernst–Planck model, J. Colloid Interface Sci. 215 (1999) 1–8.
[65] O. Truc, J.-P. Ollivier, L.-O. Nilsson, Numerical simulation of multi-species transport through saturated concrete during a migration test—MsDiff code, Cem. Concr. Res. 30 (2000) 1581–1592.
[66] M.M. Jensen, B. Johannesson, M.R. Geiker, Framework for reactive mass transport: phase change modeling of concrete by a coupled mass transport and chemical equilibrium model, Comput. Mater. Sci. 92 (2014) 213–223.
[67] B.H. Oh, S.Y. Jang, Prediction of diffusivity of concrete based on simple analytic equations, Cem. Concr. Res. 34 (2004) 463–480.